LIGHT-RESPONSIVE SELF-ASSSEMBLED MATERIALS BY SUPRAMOLECULAR POST-FUNCTIONALIZATION VIA HYDROGEN BONDING OF AMPHIPHILIC BLOCK COPOLYMERS

Alberto Concellón,[†] Eva Blasco,[‡] Alfonso Martínez-Felipe,[§] Juan Carlos Martínez,[≠] Igor Šics,[≠] Tiberio A. Ezquerra,[‖] Aurora Nogales,[‖,] Milagros Piñol[†,*] and Luis Oriol[†,*]*

[†] Departamento de Química Orgánica, Instituto de Ciencia de Materiales de Aragón (ICMA)-Facultad de Ciencias, Universidad de Zaragoza-CSIC, 50009, Zaragoza, Spain

[‡] Preparative Macromolecular Chemistry, Institut für Technische Chemie und Polymerchemie, Karlsruhe Institute of Technology (KIT), Engesserstr. 18, 76128 Karlsruhe, Germany

[§] School of Engineering, University of Aberdeen. King's College, Aberdeen AB24 3UE, UK.

[≠] Cells-Alba, Carretera, BP 1413, 08290 Cerdanyola del Vallès, Barcelona, Spain

[‖] Instituto de Estructura de la Materia, IEM-CSIC, C/Serrano 121, 28006 Madrid, Spain

* Authors for correspondence: *aurora.nogales@csic.es*, *mpinol@unizar.es*, *loriol@unizar.es*

ABSTRACT

A new class of light-responsive supramolecular amphiphilic block copolymers (BCs) based on the association through multiple H-bond between 4-isobutyloxyazobenzene motifs and 2,6-diacylaminepyridine units is reported. A block copolymer containing 2,6-diacylaminopyridine side units, in which poly(ethylene glycol) was used a hydrophilic segment, was functionalized with either a carboxylic acid azodendron, *via* double H-bonding, or a thymine azobenzene, *via* triple H-bonding. The structural and thermal characterization of these supramolecular azo-copolymers in bulk and in solution is presented. Major emphasis has been made on studying the self-assembly of these supramolecular polymers in water and their performance under UV-light by UV-vis spectroscopy, dynamic light scattering (DLS), transmission electron microscopy (TEM), and synchrotron small-angle X-ray (SAXS). This noncovalent post-polymerization functionalization strategy has provided stable self-assemblies in water with light responsive properties that can be used to load and light triggered deliver of small fluorescent molecules.

INTRODUCTION

The design of efficient drug delivery vehicles is a true challenge in polymer and materials science. A variety of polymeric nanocarriers have been described in recent years based on the ability of amphiphilic block copolymers (BCs) to spontaneously generate assemblies in water such as micelles or vesicles whose size and morphology is highly dependent on the composition, molecular geometry and relative block lengths of the BCs.[1-5] The incorporation of pH-, temperature- or light-responsive moieties into these amphiphilic BCs makes them potentially useful as systems for controlled release.[6-8] From all the stimuli, the advantage of using light as external stimulus is the possibility to apply a temporal and spatial control in the material response.[9-12] Because of the rapid, reversible, and high quantum yield photoisomerization, azobenzene is undoubtedly the most widely investigated group in the design of light-responsive systems based on amphiphilic BCs.

For some time, we have focused our interest on photoresponsive vesicles based on amphiphilic linear-dendritic (LD) BCs with a hydrophilic/hydrophobic weight ratio of approx. 20/80 using the 4-cyanoazobenzene photoresponsive moiety.[13] Theoretical simulations on these systems predicted the disruption of macromolecular aggregates by photoisomerization thus facilitating the release of encapsulated molecules.[14] Alternatively, the 4-alkoxyazobenzene photoresponsive unit was used because the presence of an alkoxy group instead a cyano at the *para*-position of the azobenzene facilitates the disruption of the assemblies under UV irradiation.[15] The vesicles were loaded with both hydrophobic and hydrophilic fluorescent probes to demonstrate that the distortion of the bilayer membrane under low intensity UV irradiation increases its permeability to the encapsulated molecules.[16, 17] These light-responsive vesicles were obtained from covalent

polymeric systems, and the frequently time-consuming synthetic procedures required to produce the polymers might reduce its practical feasibility in controlled drug release.[18, 19]

With the introduction of supramolecular polymers by Kato and Fréchet,[20] and Lehn and coworkers,[21] the playground for polymer chemists has been broadened, thus it is not restricted to macromolecular species based on the repetition of monomeric units governed by covalent bonding. Supramolecular polymeric materials combine many of the attractive features of conventional covalent polymers with the properties resulting from the reversibility of the supramolecular interactions.[22-25] In this context, several works based on noncovalent azobenzene-containing polymers have been reported. Bazuin and coworkers grafted azobenzene derivatives by ionic interactions to methylated poly(4-vinylpyridine) to obtain liquid crystalline polyelectrolytes.[26] Ionic interactions were also exploited by Marcos and coworkers for the preparation of azobenzene containing poly(propyleneimine) codendrimers by simple acid-base titration.[27-29]

Alternatively, the use of hydrogen bonding is very attractive as it combines easy preparation together with high specificity and directionality between components. Priimagi and coworkers have pioneered research on hydrogen bonded supramolecular side chain azopolymers based on poly(4-vinylpyridine) complexed with a variety of azobenzene molecules.[30-34] The strategy has also been used with supramolecular block copolymers (BCs) leading materials with multiple-level hierarchical self-assembly. Therefore, we investigated a series of photo-responsive supramolecular polymers prepared by blending carboxylic terminated promesogenic azobenzene derivatives and commercially available poly(styrene)-*block*-poly(4-vinylpyridine) copolymers in which the azo chromophore was linked to the polymer *via* hydrogen bonding.[35, 36] In these systems, the formation of supramolecular complexes takes place through molecular recognition

between the carboxylic groups (H-donor) and the pyridine rings (H-acceptor). However, even though the materials exhibited good photoresponsive properties, when high levels of complexation were required (i.e. 100% modification of the pyridine pendant units) some degree of segregation of the components was observed at the macroscopic level. Nevertheless, we have reported that this limitation can be overcome in diblock copolymers having a poly(methyl methacrylate) block and a polymethacrylate with 2,6-diacylaminopyridine pendant moieties. 2,6-Diacylaminopyridine is capable of forming multiple hydrogen bonds and, as a consequence, it was possible to reach quantitative complexation with 4-cyanoazobenzene derivatives, with no evidence of macrosegregation of the components.[37]

Recently, we have described the preparation and self-assembly of analogous amphiphilic BCs and described its potential as polymeric-based nanocarriers for hydrophobic drugs.[38] These amphiphilic BCs consisted of the polymethacrylate block bearing pendant 2,6-diacylaminopyridine units (**PDAP**) and a poly(ethylene glycol) block (**PEG**) of two different average molar masses, 2000 and 10000 g mol^{-1} (**PEG_2-*b*-PDAP** and **PEG_{10}-*b*-PDAP**, respectively) (**Figure 1a**). Polymeric micelles were prepared from these block copolymers that were used to load camphtothecin, an effective antiviral against Hepatitis C virus (HCV) by simply physical diffusion. The cytotoxicity and antiviral activity against HVC of the camphtothecin-loaded polymeric micelles were tested thus demonstrating the possibility of using these polymers for drug delivery.

Due to the ability of the 2,6-diacylaminopyridine moiety to form multiple hydrogen bonds and encouraged by the possibility of simplifying the preparation of light-responsive nanocarriers, we report this time on new amphiphilic supramolecular BCs, obtained by complexation of **PEG_2-*b*-PDAP** and **PEG_{10}-*b*-PDAP** with two 4-isobutyloxyazo derivatives, **$dAZO_i$** and **$tAZO_i$**. **$dAZO_i$**

is a dendron that contains three peripheral 4-isobutyloxyazobenzene moieties and a carboxylic acid focal point, while **tAZO$_i$** contains a thymine head linked to one 4-isobutyloxyazobenzene unit (**Figure 1b**). The 2,6-diacylaminopyridine pendant groups are able to complex the azobenzene derivatives forming either two (**dAZO$_i$**) or three (**tAZO$_i$**) hydrogen bonds (**Figure 1c**). The work describes the preparation, characterization and thermal properties of these new light-responsive, amphiphilic supramolecular polymers. As the work was motivated by the formation of assemblies in water, it also presents the characterization of the assemblies by transmission electron microscopy (TEM), dynamic light scattering (DLS) and synchrotron small-angle X-ray (SAXS), the light-responsive behavior and encapsulation-release study using fluorescent probes.

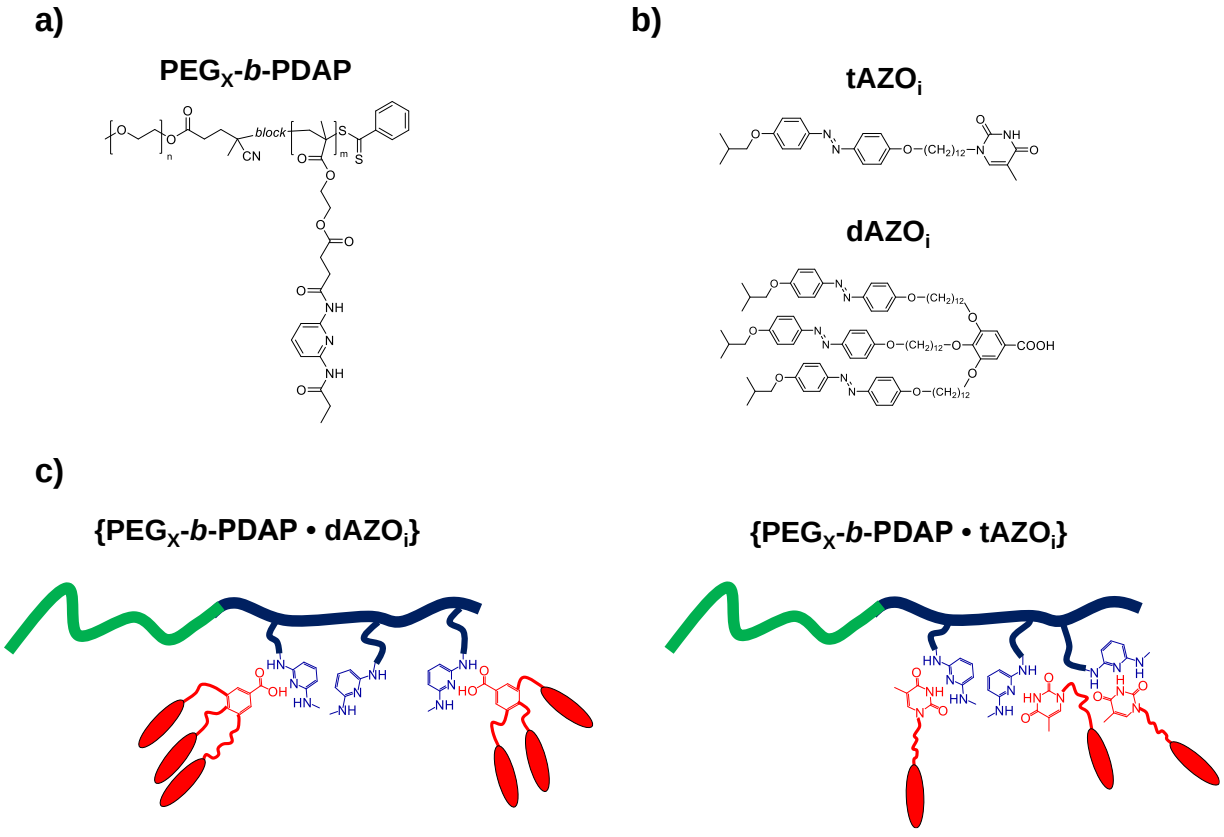

Figure 1. Chemical structure of (a) **PEGx-*b*-PDAP** block polymers, (b) **tAZOi** and **dAZOi** compounds and, schematic representation of **(c)** azobenzene-containing supramolecular BCs.

EXPERIMENTAL SECTION

Materials. **PDAP** homopolymer and **PEGx-*b*-PDAP** amphiphilic block copolymers were previously prepared.[37, 38] Details of the synthesis and characterization of **tAZOi**. **dAZOi** can be found in the Supporting Information.

Preparation of supramolecular polymers. The required amounts of the polymer and the azocompound were weighted and dissolved in THF followed by slow evaporation under stirring at room temperature. The supramolecular polymers were dried under vacuum at 40 ºC for at least 2 days. For characterization in the bulk, polymers were first heated up to 175ºC for 5 min and rapidly quenched to room temperature to have a controlled thermal history.

Preparation of self-assemblies in water. Milli-Q water was gradually added to a solution of 5 mg mL^{-1} of the corresponding BC in THF while the self-assembly process was followed by measuring the loss of intensity of transmitted light at 650 nm due to scattering (turbidimetry) as a function of the water content. At a critical water value, a sudden increase of turbidity occurs that is when the polymer self-assembly starts. When a turbidity constant value was reached, the mixture was dialyzed against water to remove THF using a Spectra/Por® dialysis membrane (MWCO 1000) for 4 days. Water suspensions of the polymers self-assemblies were obtained with a concentration around 1.7 mg mL^{-1}.

Determination of the Critical Agregation Concentration (CAC). Critical aggregation concentration (CAC) was determined by fluorescence spectroscopy using Nile Red as the probe as follows: 119 μL of a solution of Nile Red in dichloromethane (5×10^{-6} M) was added into a series of flasks and then the solvent evaporated. Afterwards, a water suspension of the self-assemblies was added to each flask with concentration ranging from 1.0×10^{-4} to 1.0 mg mL^{-1}. The suspension was prepared by diluting the former 1.7 mg mL^{-1} suspension. In each flask a final concentration of 1.0×10^{-6} M of Nile Red was reached. The suspensions were stirred overnight at room temperature to reach equilibrium before fluorescence was measured. The emission spectra of Nile Red were registered from 560 to 700 nm while exciting at 550 nm.

Loading of Rhodamine B into the vesicle. Vesicles formation was carried out following the procedure described for the formation of self-assemblies but using a solution of Rhodamine B in Milli-Q water. The BC was dissolved in THF and the aqueous solution of Rhodamine B was gradually added. The charge ratio was 1:5 mol copolymer/mol dye. Self-assembly was followed by turbidimetry until an almost constant value was reached. Finally, the mixture was dialyzed against water to remove THF and non-encapsulated Rhodamine B. The absorbance of the dialyzed solution was measured. Measured absorptions were compared with a calibration curve of the Rhodamine B previously obtained, that allowed to determine the quantity of non-encapsulated dye molecules and therefore the number of molecules encapsulated in the vesicle.

Irradiation experiments. The water dispersions of self-assemblies were irradiated with a compact low-pressure fluorescent lamp Philips PL-S 9W emitting between 350 and 400 nm. The samples were placed at a distance of 10 cm from the light source in quartz cuvettes at room temperature. After irradiation, the water suspensions were kept in dark.

Techniques. FTIR spectra were obtained on a Bruker Vertex 70 FT-IR spectrophotometer using KBr pellets. Solution NMR experiments were carried out on Bruker Avance spectrometers operating at 400 or 300 MHz for ^{1}H and 100 or 75 for ^{13}C, using standard pulse sequences. Chemical shifts are given in ppm relative to TMS and the solvent residual peak was used as internal reference. Thermogravimetric analysis (TGA) were performed using a Q5000IR from TA instruments at heating rate of 10 ºC min^{-1} under a nitrogen atmosphere. Thermal transitions were determined by differential scanning calorimetry (DSC) using a DSC Q2000 from TA instruments with powdered samples (2−5 mg) sealed in aluminum pans. Glass transition temperatures (T_g) were determined at the half height of the baseline jump, and first order transition temperatures were read at the maximum of the corresponding peak for the polymers and at the onset for low molar mass compounds. Homogeneity of the samples was inspected by polarizing optical microscopy (POM) using an Olympus BH-2 polarizing microscope fitted with a Linkam THMS600 hot stage. UV-Vis absorption spectra were recorded on an ATI-Unicam UV4-200 spectrophotometer. Fluorescence measurements were performed using a Perkin Elmer LS 50B fluorescence spectrophotometer. Dynamic light scattering (DLS) measurements were carried out on a Malvern Instrument Nano ZS using a He–Ne laser with a 633 nm wavelength, a detector angle of 173º at 25 ºC using a He–Ne laser with a 633 nm wavelength. The self-assemblies concentrations were 0.075 mg mL^{-1} and size measurements were performed at least three times on each sample to ensure consistency.

Transmission electron microscopy (TEM) and cryoscopic transmission electron microscopy (Cryo-TEM). The morphological study of the block copolymer vesicles was carried out by transmission electron microscopy (TEM) using a JEOL-2000 FXIII and TECNAI G^2 20 (FEI COMPANY) electron microscope operating at 200 kV. *Preparation of samples for*

TEM inspection: 5 μL of a 0.5 mg mL^{-1} water dispersion of the self-assemblies was deposited onto carbon-coated copper grid. Water of the sample was removed by capillarity using filter paper. Then, the sample was stained with uranyl acetate and the grid was left to dry overnight under vacuum. The 0.5 mg mL^{-1} suspension was prepared by diluting the former 1.7 mg mL^{-1} suspension with Milli-Q water.

Cryo-TEM was performed using a JEM-2011 electron microscope on samples rapidly frozen in liquid ethane. *Preparation of Samples for Cryo-TEM Inspection:* 5 μL of a 1.7 mg mL^{-1} water dispersion of self-assemblies were applied to a suitable grid and then rapidly frozen in liquid ethane.

Confocal Microscopy. Samples were observed with an Olympus FV10i confocal scanning microscope. Images were collected using a 60× oil immersion lens (lens specification, Plan S-APO 60×O, NA 1.35), a line average of 8 and a format of 1024×1024 pixels. The confocal pinhole was 1 Airy unit. *Sample Preparation:* 5 μL of a 1.7 mg mL^{-1} water dispersion of self-assemblies with encapsulated Rhodamine B were applied to a glass slide and a cover slip was placed on the top of the sample. The edges were sealed to avoid solvent evaporation during measurement.

Small Angle X-Ray Scattering (SAXS). X-ray scattering techniques provide information about the structure and molecular conformations at different length scales. SAXS allows one to analyze the structure developed over the length scale of tens of nanometers and it is of particular value when studying supramolecular organization.[39] Synchrotron radiation offers the possibility to follow by SAXS and WAXS real time changes in both the conformation and the structure.[40] Experiments were performed at beamline BL11-NCD (ALBA, Spain) using a wavelength of 0.1

nm. The SAXS detector (ADSC, Quantum 210r CCD, pixel size 102 μm) was located at 6430 mm distance from the sample position. Experiments under UV irradiation were performed at room temperature in the following way: SAXS patterns were collected while the sample was irradiated with a UV lamp (Phillips PL-S 9W) placed at a distance of 10 cm. The angular (q-axis) calibration was obtained by measuring standard samples of Silver Behenate.

RESULTS AND DISCUSSION

Preparation and characterization of supramolecular polymers. Supramolecular block polymers were prepared by solving the corresponding amounts of the parent BCs (**PEG$_x$-*b*-PDAP**) and the azocompounds (**dAZO$_i$** or **tAZO$_i$**) in THF, followed by slow evaporation of the solvent under continuous stirring at room temperature. According to our previous results on covalent LDBCs, the degree of complexation (number of azo molecules per 2,6-diacylaminopyridine repeating unit) was adjusted to achieve hydrophilic/hydrophobic weight ratios of approx. 20:80 because for this value vesicles were predominantly observed.[13] Therefore, a degree of complexation of 1 was used with **tAZO$_i$**, while 0.30 was used with **dAZO$_i$** (see **Table 1**). For comparative purposes, fully complexed supramolecular polymers (degree of complexation=1) of the homopolymer **PDAP**[37] with either **dAZO$_i$** or **tAZO$_i$** were also prepared.

The ^{1}H NMR spectra of the supramolecular BCs were recorded on $CDCl_3$ and demonstrated the formation of hydrogen bonded complexes, assuming that there is a rapid equilibrium between the complex and its components. In general, proton signals involved in the hydrogen bond, and those that are close to the complexing groups experienced correlated changes in their chemical

shifts. As a representative example, the ^{1}H NMR spectra of the {**PEG$_2$-*b*-PDAP•tAZO$_i$**} and {**PEG$_2$-*b*-PDAP•dAZO$_i$**} supramolecular polymers are shown in **Figure 2**, along with those of their components. On the {**PEG$_2$-*b*-PDAP•tAZO$_i$**} spectrum, N–H proton signals (H_A) of the PDAP block were shifted downfield (from 8.45 to 9.23 ppm) as well as the thymine N–H group signals (H_B) of the **tAZO$_i$** (from 8.25 to 9.71 ppm), indicating the hydrogen bond formation between complementary **tAZO$_i$** and 2,6-diacylaminopyridine units. In the case of supramolecular BCs containing **dAZO$_i$**, the 2,6-diacylaminopyridine N–H protons (H_A) experienced slight downfield displacement (from 8.45 to 8.58 ppm) due to hydrogen bonding interactions with the **dAZO$_i$** carboxylic acid. In this case the shift was small because of the low complexation degree of these supramolecular BCs, see **Table 1**. The acidic proton signal (H_C) was very broad and was not visible in the ^{1}H NMR spectrum. It is particularly noteworthy that in both cases the protons close to the hydrogen bonds experienced slight displacements. For example, protons of the pyridine ring of the 2,6-diacylaminopyridine units (H_{PY}) are shifted by around +0.05 ppm. NOESY experiments in $CDCl_3$ were also performed to determine whether hydrogen bonding interactions are established between the 2,6-diacylaminopyridine units and **tAZO$_i$** or **dAZO$_i$**. The ^{1}H–^{1}H NOESY spectrum of **{PEG$_2$-*b*-PDAP•tAZO$_i$}** is shown in **Figure S6**. Significant cross-peaks were observed between H_A and H_B, indicating that these groups are close in space because of H-bonding interactions. However, NOESY experiments of BCs with **dAZO$_i$** did not show any additional information.

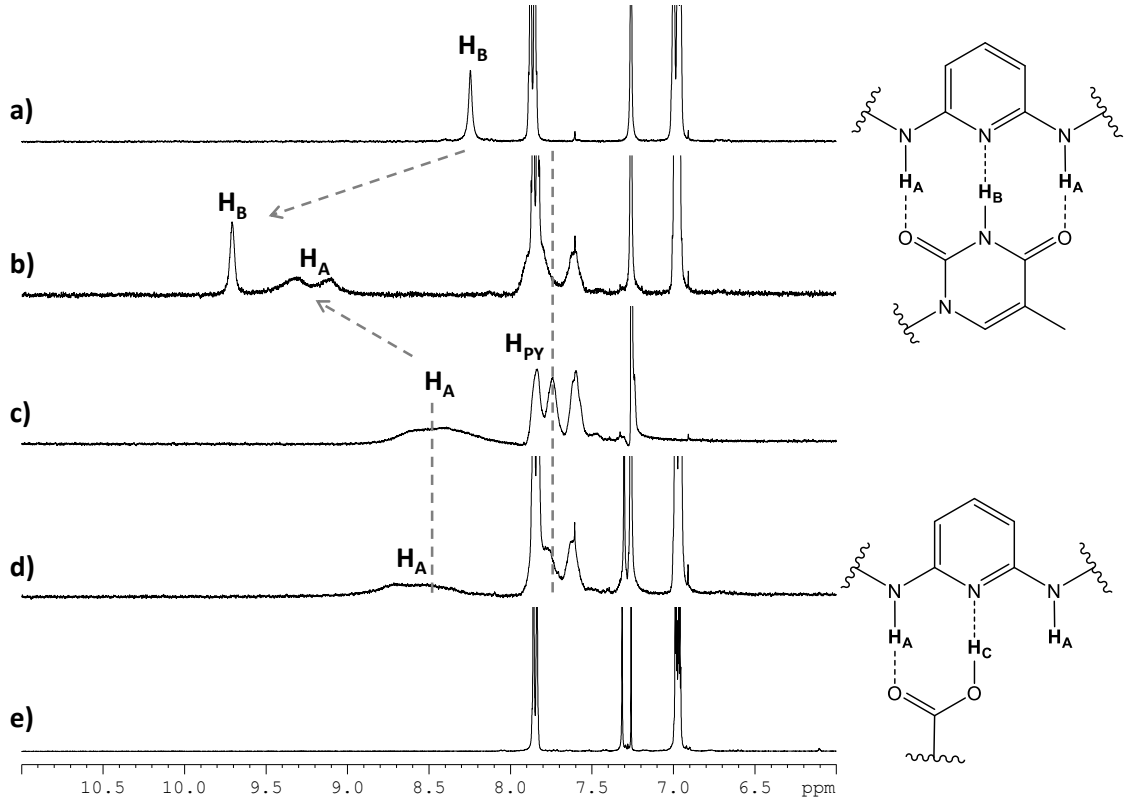

Figure 2. ^{1}H NMR spectra of (a) **tAZO$_i$**, (b) **{PEG$_2$-*b*-PDAP•tAZO$_i$}**, (c) **PEG$_2$-*b*-PDAP**, (d) **{PEG$_2$-*b*-PDAP•dAZO$_i$}**, and (e) **dAZO$_i$**, in $CDCl_3$ solution at 25ºC.

Temperature dependent NMR experiments can also provide valuable information about hydrogen bonding interactions. Therefore, ^{1}H NMR spectra were recorded in solution at different temperatures (**Figure 3**). On heating **tAZO$_i$** complexes, H_A and H_B signals moved steadily upfield from 9.23 and 9.71 to 8.95 and 9.01 ppm, respectively. In **dAZO$_i$** complexes, H_A signal also moved upfield from 8.61 to 8.36 ppm when the temperature increased from 25 to 55 ºC. The gradual upfield displacements are attributed to the dissociation of the hydrogen bonds on increasing the temperature. When solutions were cooled from 55 to 25 ºC, all upfield displaced signals went back to its original chemical shifts. These results indicate the thermoreversible hydrogen bond formation between complementary units.[41]

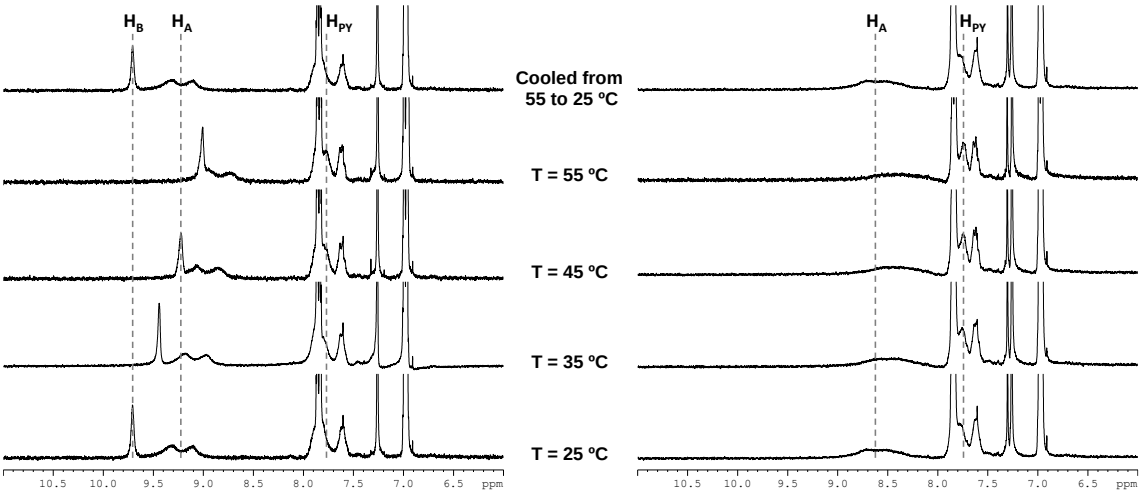

Figure 3. ^{1}H NMR spectra in $CDCl_3$ solution of **{PEG$_2$-*b*-PDAP•tAZO$_i$}** (left) and **{PEG$_2$-*b*-PDAP•dAZO$_i$}** (right) taken at different temperatures (bottom to top: spectra registered on heating and after cooling down again to room temperature).

The IR spectra of the complexes display several changes, respect to the azocompounds and polymer precursors, due to the formation of specific interactions between the PDAP units and the azocompounds. An overview of the spectra in the complete frequency range of {**PDAP•tAZO$_i$**} and {**PDAP•dAZO$_i$**} along with their precursors is shown in **Figure S7** (Supporting Information). In the case of supramolecular polymers containing **tAZO$_i$** (**Figure S8a**), significant modifications of the C=O*st*, N–H*st* and N–Hδ bands, suggest that the N–H groups of the 2,6-diacylaminopyridine cores are forming hydrogen bonds with the thymine units. The temperature variable IR profiles do not vary to a great extent, as a consequence of the stability of these interactions in the bulk, and only slight variations are observed in the C=O*st* and N–Hδ regions, (see **Figure S9a**). The C=O*st* region of **dAZO$_i$** complexes (**Figure S8b),** show two main bands at around 1690 cm^{-1} (**dAZO$_i$** hydrogen bonded acid groups and amide groups of 2,6-diacylaminopyridine) and 1730 cm^{-1} (ester and free **dAZO$_i$** acid groups). On heating above the

melting temperature (**Figure S9b)**, the 1690 cm^{-1} region undergoes a relative decrease while the 1730 cm^{-1} band broadens, and this accompanied with a noticeable decrease of the N–H*st* signals (below 3400 cm^{-1}). These simultaneous variations indicate partial breakage of hydrogen bonds between the acid groups of **dAZO$_i$** and the amide groups of the 2,6-diacylaminopyridine cores. These changes are reversed on cooling, and the behavior is reproducible on further heating and cooling cycles.

Thermal Characterization of Precursors and Supramolecular BCs. Azocompound precursors and derived supramolecular polymers showed good thermal stability as determined by TGA with onset temperatures (T_{onset}) associated to mass loss above 200ºC (**Table 1**). Evolution of volatiles due to the presence of residual solvents or water was not observed. The thermal behavior of the building components and of the supramolecular polymers was evaluated by DSC (**Table 1**). Properties of **PDAP** homopolymer, the PEG macro-CTAs, **PEG$_X$-CTA**, and **PEG$_X$-*b*-PDAP** BCs were previously reported[38] and relevant data are included in **Table 1** as reference**.** BCs **PEG$_X$-*b*-PDAP** are amorphous materials and only exhibit a single T_g (no melting transitions were observed) indicating compatibility between blocks. The low molar mass azocompound **tAZO$_i$** is a crystalline material that melts to give an isotropic liquid phase at 166ºC while **dAZO$_i$** exhibits semicrystalline behavior, showing a glass transition T_g at 68ºC and a T_m at 141ºC (see **Figure S10** in Supporting Information).

All the supramolecular polymers appear as homogeneous under POM, with no signs of segregation of the individual components upon several heating and cooling cycles, indicating the formation of a single-like and homogeneous material. Complexation by hydrogen bonding promotes notable variations in the thermal properties of the **tAZO$_i$**-containing supramolecular polymers compared to the polymer and the azocompound precursors (**Figure 4**). On heating,

{PDAP•tAZO$_i$}, prepared as reference, displays a T_g at around 35ºC followed by cold crystallization and subsequent melting of the crystalline complexed PDAP block at 148 ºC (**Figure 4**, trace **a**). On the DSC curves of **{PEG$_X$-*b*-PDAP•tAZO$_i$}** (**Figure 4**, traces **b** and **c**), melting of the PEG block is additionally observed just above (and overlapping) the T_g of the complexed PDAP block, at 40−48 ºC. The appearance of several thermal events ascribable to the different blocks suggests that complexation induces microphase separation by decreasing the miscibility between blocks.

The **dAZO$_i$**-containing homopolymer, **{PDAP•dAZO$_i$},** is a semicrystalline material with glass and melting transitions at 77 ºC and 136 ºC, respectively, (**Figure 5**, trace **a**). The supramolecular BCs, **{PEG$_X$-*b*-PDAP•dAZO$_i$}**, also show an additional glass transition at lower temperatures, around 4-15ºC, together with a weak thermal event related to melting of the PEG blocks at 40-52ºC (see inset in **Figure 5**). These results seem to confirm again that complexation promotes microphase separation similarly to the **tAZO$_i$** containing BCs. The appearance of the T_g at lower temperatures (T_g ~ 4-15ºC) can be explained by the low complexation degree of these two samples (degree of complexation = 0.30), which leads to the observation of the T_g corresponding to **PEG$_X$-*b*-PDAP** (uncomplexed).

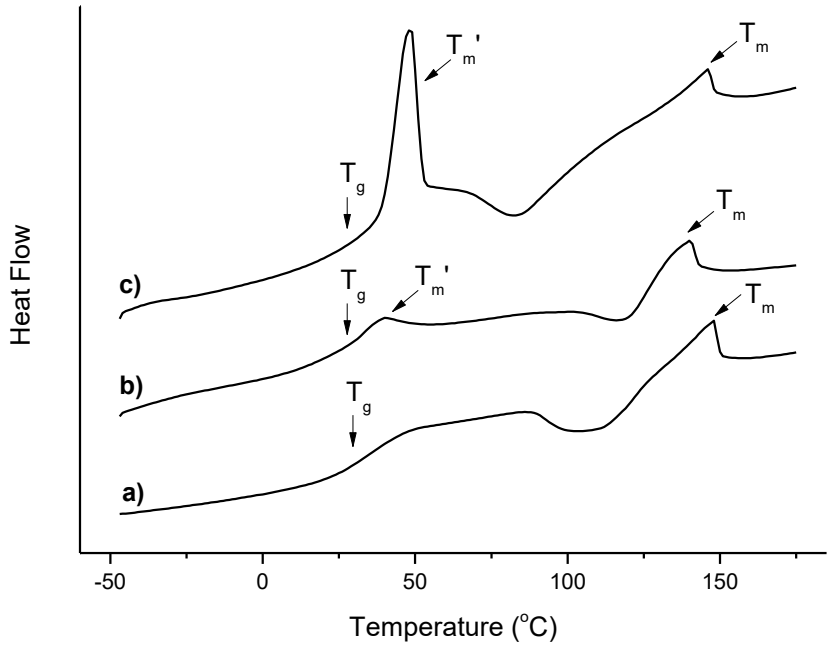

Figure 4. DSC traces of (a) **{PDAP•tAZO$_i$}**, (b) **{PEG$_2$-*b*-PDAP•tAZO$_i$}** and (c) **{PEG$_{10}$-*b*-PDAP•tAZO$_i$}** corresponding to the second heating scan (10 ^{o}C min^{-1}, Exo down)

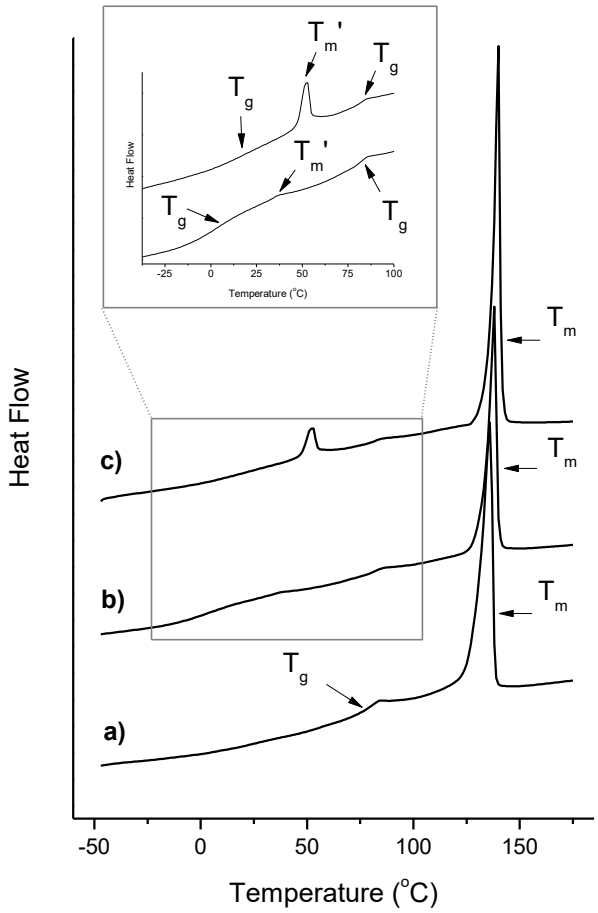

Figure 5. DSC traces of (a) **{PDAP•dAZO$_i$}, (b) {PEG$_2$-*b*-PDAP•dAZO$_i$} and (c) {PEG$_{10}$-*b*-PDAP•dAZO$_i$}** corresponding to the second heating scan (10 ºC min^{-1}, Exo down)

Self-Assembly of the supramolecular BCs in water. Self-assembled structures of the supramolecular BCs were prepared by the co-solvent method using THF/water and the process was monitored following the increase of turbidity under water addition (see **Figure S11** in Supporting Information). It was previously described that **PEG$_X$-*b*-PDAP** form spherical micellar self-assemblies with a diameter of approx. 21 nm for **PEG$_2$-*b*-PDAP** and 32 nm for **PEG$_{10}$-*b*-PDAP** as determined by DLS (18 and 25 nm as determined by TEM).[38] **dAZO$_i$-**

containing supramolecular BCs precipitated during dialysis, which points to the collapse of the assemblies in water. Nevertheless, stable dispersions on storing for a few weeks were obtained for **tAZO$_i$** containing supramolecular BCs. Because of this, any further study was limited to **{PEG$_2$-*b*-PDAP•tAZO$_i$}** and **{PEG$_{10}$-*b*-PDAP•tAZO$_i$}**.

The CAC of **{PEG$_2$-*b*-PDAP•tAZO$_i$}** and **{PEG$_{10}$-*b*-PDAP•tAZO$_i$}** in water, as the concentration of the amphiphilic polymer above which the polymer chains start to associate, was determined by fluorescence using Nile Red (**Figure S12** in Supporting Information). Calculated CAC values, which correlate the thermodynamic stability, were 28 and 42 μg/mL for **{PEG$_2$-*b*-PDAP•tAZO$_i$}** and **{PEG$_{10}$-*b*-PDAP•tAZO$_i$}**, respectively. These values are typical for amphiphilic BCs.[42]

The morphology of the self-assemblies was first investigated by TEM and it was found that **{PEG$_2$-*b*-PDAP•tAZO$_i$}** self-assembled into vesicles with a deflated appearance because of water removal during the sample preparation for TEM inspection (**Figure 6a**). The aqueous suspension of the vesicles was inspected by cryo-TEM without the need of staining; in this case, the sample was vitrified in liquid ethane at −170 ºC. Cryo-TEM images showed spherical vesicles having a membrane thickness around 10 nm (**Figure 6b**). The mean average hydrodynamic diameter (D_h) of these vesicles evaluated by DLS was 345 nm (**Figure 7**), which is in good agreement with cryo-TEM observations. It is worth emphasizing that parent **PEG$_2$-*b*-PDAP** formed spherical micelles and upon functionalization via H-bonding with **tAZO$_i$**, vesicles are formed.

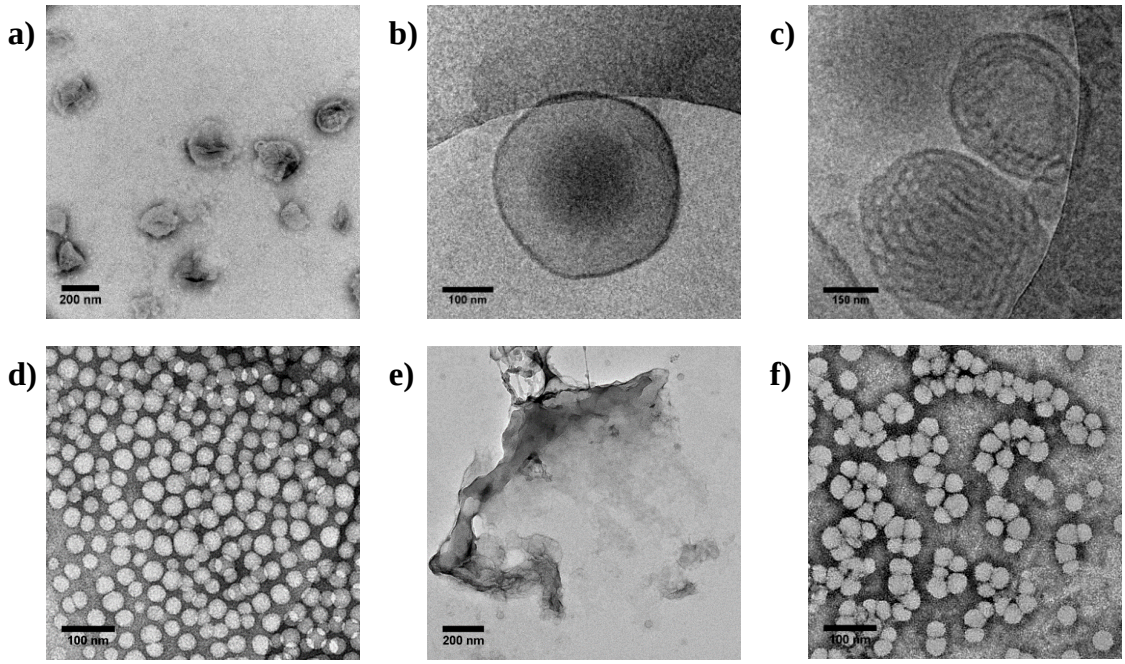

Figure 6. TEM image of (a) **{PEG$_2$-*b*-PDAP•tAZO$_i$}** non-irradiated vesicles. Cryo-TEM images of **{PEG$_2$-*b*-PDAP•tAZO$_i$}** vesicles (b) before and (c) after UV irradiation**.** TEM images of **{PEG$_{10}$-*b*-PDAP•tAZO$_i$}** micelles (d) before, (e) after irradiation and (f) 24h after irradiation.

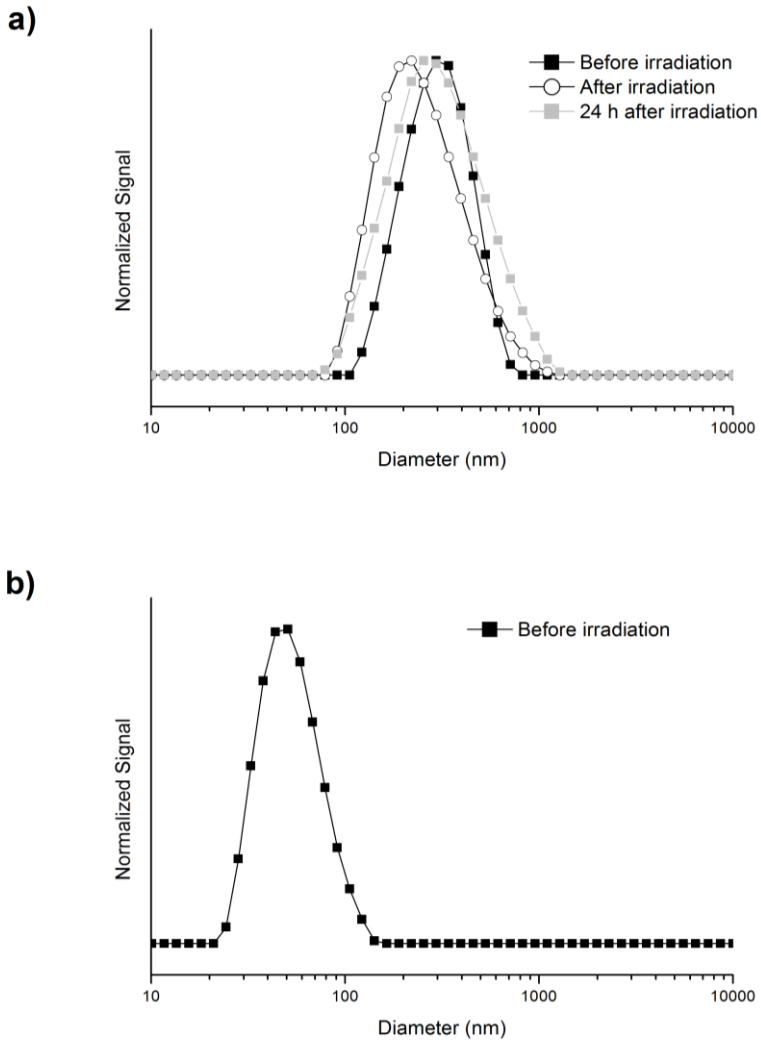

Figure 7. DLS measurements of a water suspension of (a) **{PEG$_2$-*b*-PDAP•tAZO$_i$}** vesicles before and after irradiation for 10 min and (b) **{PEG$_{10}$-*b*-PDAP•tAZO$_i$}** non-irradiated micelles (after irradiation, accurate DLS measurements were not possible).

TEM images of **{PEG$_{10}$-*b*-PDAP•tAZO$_i$}** show the formation of spherical micelles with a diameter of approx. 40 nm (**Figure 6d**). The average D_h determined by DLS was 51 nm (**Figure 7**). However, in this case, **PEG$_{10}$-*b*-PDAP** complexation with **tAZO$_i$** does not produce morphological changes (from spherical micelles to vesicles) of the self-assembled structures

although larger micelles (20 nm increase on diameter) are observed as consequence of complexation. Macromolecular structure and the hydrophobic/hydrophilic balance influence on the final morphology of the supramolecular BCs. Thus, in **{PEG$_2$-*b*-PDAP•tAZO$_i$}** the hydrophilic/hydrophobic weight balance, which change from approx. 35/65 to 18/82 upon complexation, seems to be enough to stabilize the vesicular morphology while the longer molecular weight of the blocks in **{PEG$_{10}$-*b*-PDAP•tAZO$_i$}** seems to stabilize the spherical micellar morphology under these experimental conditions.

Light-responsive behavior of the supramolecular BCs. The photoresponse of **{PEG$_2$-*b*-PDAP•tAZO$_i$}** and **{PEG$_{10}$-*b*-PDAP•tAZO$_i$}** was first evaluated by UV-vis spectroscopy. The spectra of the amphiphilic BCs in THF solution showed an intense band at 362 nm related to the π-π* transition together with a weak absorption band at about 450 nm corresponding to the symmetry forbidden n-π* transition of the *E*-isomer. The spectra of both, micelles and vesicles, in water showed a broadening and hypsochromic shift of the π-π* band (**Figure 8**) compared to the spectra of the supramolecular BCs in THF. The absorption band shifted down to 348 nm, which indicates the predominant formation of azobenzene H-aggregates. Furthermore two contributions at higher wavelengths were observed, one at 362 nm corresponding to the value determined for the non-aggregated *E*-azobenzene detected in solution and other at 378 nm characteristic of J-aggregates.

To demonstrate the sensitivity of the self-assemblies to UV-light, the assemblies suspensions were UV illuminated while changes in the UV-vis spectra were recorded (**Figure 8**). A remarkably decrease of π-π* absorbance was observed accompanied by a notably increase of the absorbance at 450 nm due to the photoinduced *E*-to-*Z*-azobenzene isomerization. After 10 min of light exposure, only slight changes were observed in the UV-vis spectrum indicating that a

photostationary state was reached. After 24h in the dark, UV-vis spectra started to recover the initial shape due to thermal *Z*-to-*E* back isomerization.

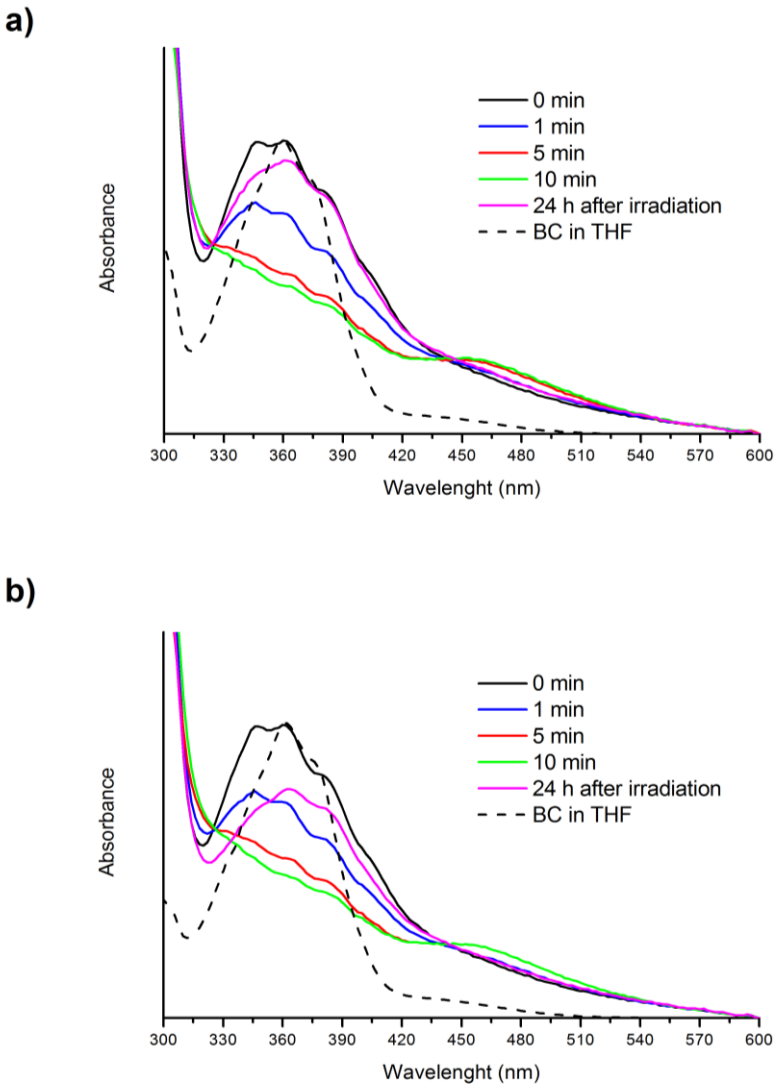

Figure 8. UV-Vis spectra of **(a) {PEG$_2$-*b*-PDAP•tAZO$_i$}** and **(b) {PEG$_{10}$-*b*-PDAP•tAZO$_i$}** in a 5×10^{-6} M THF solution and UV irradiated self-assemblies (1 mg mL^{-1} suspensions) for different times.

TEM or Cryo-TEM and DLS techniques were used to gain information about any morphological changes upon 10 min UV irradiation. For **{PEG$_2$-*b*-PDAP•tAZO$_i$}** cryo-TEM images show the presence of wrinkled vesicles (**Figure 6c**) of smaller average D_h, around 225 nm, as calculated by DLS (**Figure 7**).

TEM images of irradiated **{PEG$_{10}$-*b*-PDAP•tAZO$_i$}** micelles taken immediately after UV illumination show disruption of the assemblies and presence of material without clear morphology (**Figure 6e**). Accordingly, accurate measurements by DLS were not possible. TEM images of irradiated suspensions taken after maintaining the sample 24 h in the dark at room temperature were additionally registered. Under these conditions, thermal *Z*-to-*E* back isomerization of the azobenzene takes place and images show that micelles are at least partially recovered (**Figure 6f**).

Self-assemblies of parent **PEG$_X$-*b*-PDAP**, and of supramolecular BCs **{PEG$_X$-*b*-PDAP•tAZO$_i$}** and their light response were investigated by SAXS. **Figure 9a** shows the SAXS profile as a function of the module of the scattering vector q ($q=4\pi/\lambda sin(\theta)$, being 2θ the scattering angle) from aggregates in water. In the case of the **PEG$_X$-*b*-PDAP** BCs, SAXS curves can be described by the scattering of a distribution of spheres with different diameters.[43, 44] The scattering form factor for a sphere of radius R is given by **Eq 1**:

$$F_s(q,R) = \left[\frac{3[\sin(qR)] - qRcos(qR)}{(qR)^3}\right]^2 \quad (1)$$

For **PEG$_2$-*b*-PDAP** the distribution was centered around diameters ($2R$) of approx. 18 nm and around 25 nm for **PEG$_{10}$-*b*-PDAP** (**Figure 9b**), which are consistent with DLS analysis and TEM observations.[38]

However, the scattering from **{PEG$_x$-*b*-PDAP•tAZO$_i$}** assemblies cannot be fitted with a simple sphere distribution model. In the case of **{PEG$_2$-*b*-PDAP•tAZO$_i$}** cryo-TEM images (**Figure 6b**) showed that the assemblies are vesicles with a diameter larger than 300 nm and a wall thickness of just several nanometers. Therefore, due to the vesicle dimensions, SAXS profiles only give information about the wall of the vesicle. Considering this and using the Guinier approximation for planar objects, from the scattering curve of the supramolecular assembly **{PEG$_2$-*b*-PDAP•tAZO$_i$}** it is possible to obtain the radius of gyration (**Eq 2).** [45] The radius of gyration for a planar object with large lateral dimensions is related to its thickness (**Eq 3).**

$$I(q) \sim q^{-2} exp\left(-q^2 R_g^2\right) \quad (2)$$

$$d_t^2 = 12 R_g^2 \quad (3)$$

Figure 9c shows Guinier plot for **{PEG$_2$-*b*-PDAP•tAZO$_i$}** in the dark. From the fitting of the scattering to the Guinier approximation, a vesicle wall thickness of around 10 nm was obtained, which fits well with cryo-TEM observations (**Figure 6b**).

In order to follow the modifications induced on the morphology of the supramolecular assemblies by the UV light illumination, real time SAXS experiments were performed on the **tAZO$_i$** containing supramolecular assemblies. **Figure 10a** shows the scattering curves corresponding to **{PEG$_2$-*b*-PDAP•tAZO$_i$}** vesicles for selected UV illumination times. As observed, the UV light induced subtle changes in the scattering curves, especially at large values of q; although, these changes could not be quantified due to the noise of the measurements. Nevertheless, Guinier analysis of the curves allowed to estimate the thickness of the vesicle wall as a function of the UV exposure time. These results are presented in the inset of **Figure 10a**.

SAXS results show that the UV illumination induced changes on the vesicles wall, in particular a thinning of the wall. For long UV illumination times, the slope at low q increases indicating that aggregation took place.

The assemblies of the supramolecular polymer **{PEG$_{10}$-*b*-PDAP•tAZO$_i$}** presented a different scattering. For **{PEG$_{10}$-*b*-PDAP•tAZO$_i$}**, micelles of mean radius around 20 nm were observed by TEM. Although an estimation of the radius of the spherical objects can be obtained by the Guinier approximation, in this case, the whole scattering curve of these assemblies can be fitted using the form factor of a micelle model with a spherical core and Gaussian polymer chains attached to the surface (**Eq 4**):[46, 47]

$$F_{mic}(q) = N_{agg}^2 \rho_s^2 F_s(q,R) + N_{agg}^2 \rho_c^2 F_c\left(q, R_{gauss}\right) + N_{agg}\left(N_{agg}-1\right)\rho_c^2 S_{cc}(q) + 2N_{agg}^2 \rho_c \rho_s S_{sc}(q) \qquad (4)$$

considering the self-correlation term F_S of the spherical core, of radius R, the self-correlation of the Gaussian chains Fc, characterized by their radius of gyration R_{gauss}, and the crossed terms between the core and the Gaussian chains, S_{SC}, where the fact that the chains cannot penetrate the core is considered, and finally a crossed term between the different Gaussian chains decorating the core S_{CC}.[46] N_{agg} is the aggregation number of the micelle, i.e. the number of molecules per micelle, ρ_C and ρS are the total scattering length excess of the blocks in the spherical core and in the chains respectively.

Figure 10b shows the scattering of the **{PEG$_{10}$-*b*-PDAP•tAZO$_i$}** assemblies in water initially in the dark and after 15 min of UV illumination. Only slight changes were observed. However, fitting their scattering to **Eq 3** allowed to obtain the evolution with UV illumination time of the

relevant parameters (**Figure 10c**). As the sample was illuminated, the number of chains per micelle decreased slightly, whereas the core radius increased slightly and the radius of gyration of the chains at the surface remained nearly constant. These results can be explained considering that, because the photoresponsive **tAZO$_i$** groups are located within the core of the micelles, the effect of UV irradiation should be more significant on the core than on the shell of the micelles. Also, the decrease of the number of chains per micelle indicated that the micelles were gradually getting destroyed.

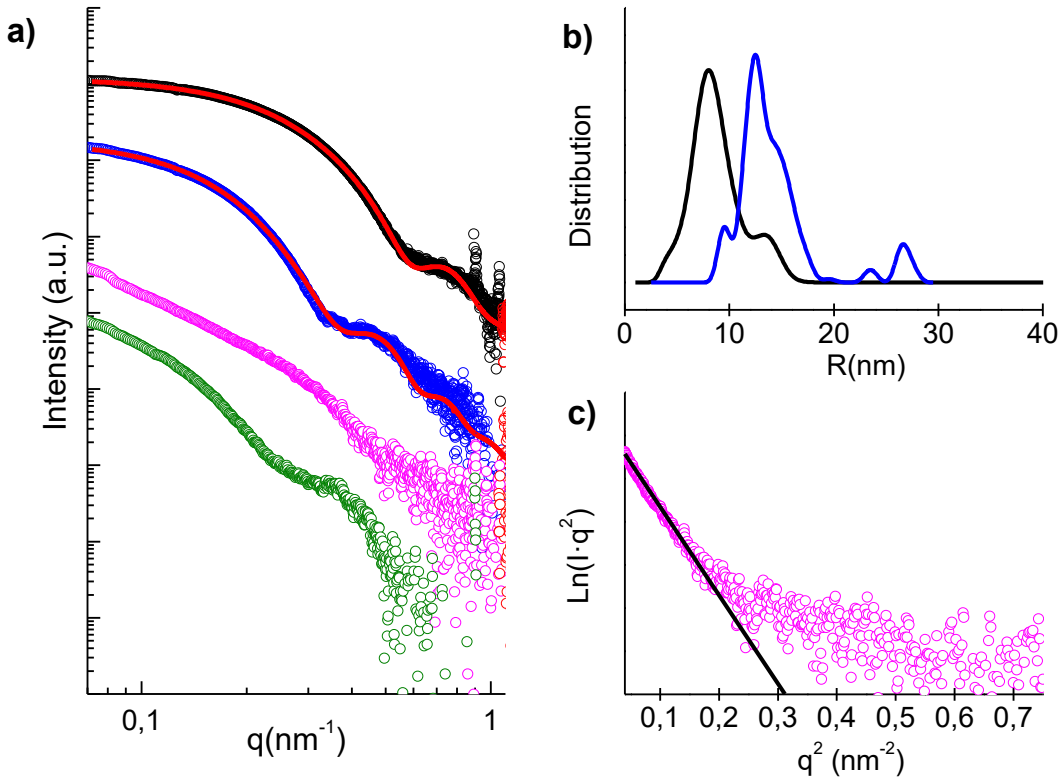

Figure 9. **(a)** SAXS profiles from **PEG$_2$-*b*-PDAP** (o), **PEG$_{10}$-*b*-PDAP** (o), **{PEG$_2$-*b*-PDAP•tAZO$_i$}** (o) and **{PEG$_{10}$-*b*-PDAP•tAZO$_i$}** (o) in dark. Continuous red lines are fits to the scattering from a distribution of individual spheres. **(b)** Radius distribution of the spheres

(according to the fit in figure a) for **PEG$_2$-*b*-PDAP** (black) and **PEG$_{10}$-*b*-PDAP** (blue). **(c)** Guinier plot of the scattering from the supramolecular polymer **{PEG$_2$-*b*-PDAP•tAZO$_i$}** in the dark. The continuous line corresponds to the fit to Eq 2.

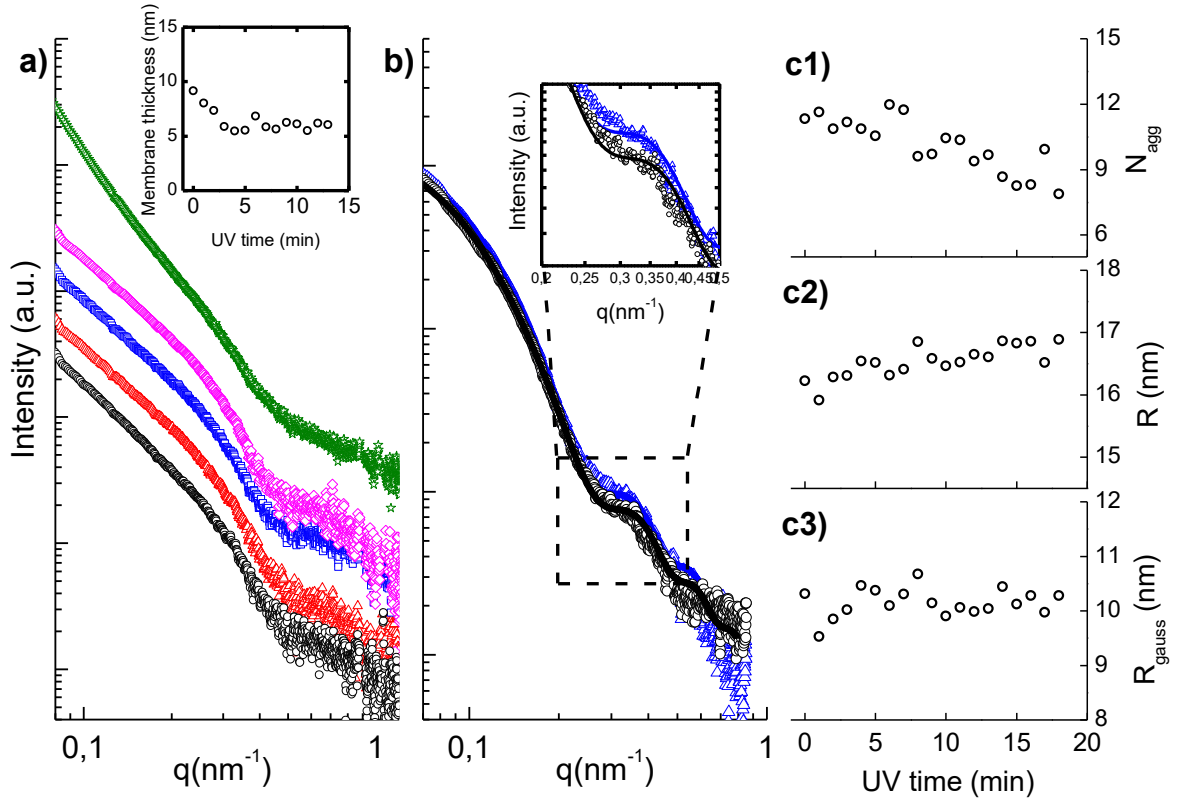

Figure 10. **(a)** SAXS profiles from **{PEG$_2$-*b*-PDAP•tAZO$_i$}** assemblies in dark (o), and after 5 (△),10 (□), 15 (◇) and 20 (☆) min of UV illumination. The inset in (a) shows the evolution of the vesicle membrane thickness as obtained by the Guinier approximation in Eq 2 and Eq 3. **(b)** SAXS profiles from **{PEG$_{10}$-*b*-PDAP•tAZO$_i$}** assemblies in dark (o) and after 15 min of UV illumination (△). Continuous lines correspond to fit to Eq 4. **(c)** Variation of the relevant structural parameters included in Eq 4 related to the micelles of **{PEG$_{10}$-*b*-PDAP•tAZO$_i$}** under

UV illumination: (c1) Number of chain per micelle, (c2) Radius of the core, and (c3) Radius of gyration of the Gaussian chains forming the shell.

Light stimulated release of fluorescence probes from supramolecular BCs. The potential of the vesicles and micelles as stimulus responsive nanocontainers was investigated by encapsulation and subsequent release of fluorescent probes. With **{PEG$_2$-*b*-PDAP•tAZO$_i$}** vesicles, two fluorescent probes were tested because molecules of interest can be trapped either into the hydrophilic hollow cavity or the hydrophobic membrane formed by the azobenzene moieties. Therefore, the ability to encapsulate Nile Red or Rhodamine B, which are respectively of hydrophobic and hydrophilic nature, was confirmed for these systems.

Nile Red loaded **{PEG$_2$-*b*-PDAP•tAZO$_i$}** show a strong emission from 560 to 700 nm while exciting at 550 nm. Upon irradiation, an abrupt decrease on the initial fluorescence intensity at 606 nm was observed (**Figure 11a**), which indicated a change to a less hydrophobic surrounding. This can be due to Nile Red migrating from the membrane to the aqueous media and also to the increase in the polarity in the inner membrane due to photoisomerization.[16] When the irradiated vesicles were kept in the dark for 24 h, the fluorescence was partially recovered, which could be related with a partial release of the fluorescent probe.

{PEG$_2$-*b*-PDAP•tAZO$_i$} vesicles were loaded with Rhodamine B when forming the vesicles in the presence of the probe, and it was estimated that 0.8 molecules of Rhodamine B were trapped per macromolecule of BC (using a feed ratio of 5:1 Rhodamine/macromolecule). Rhodamine B encapsulation was confirmed by confocal microscopy images where fluorescence dots in a dark background were observed (**Figure 12a**). After 10 min of UV light irradiation, fluorescence dots were still visible but the fluorescence of background was more intense due to

Rhodamine B release from the interior of the vesicles to the aqueous surrounding media (**Figure 12b**) proving that the vesicle membrane became permeable to the probe after UV irradiation.

{PEG$_{10}$-*b*-PDAP•tAZO$_i$} micelles were only loaded with Nile Red which should be accommodate within their hydrophobic cores. Again, an abrupt decrease of the initial fluorescence was observed after UV irradiation, indicating that the environment of the probe becomes more hydrophilic (**Figure 11b**). After 24h, the Nile Red fluorescence was not completely recovered, pointing to that part of the Nile Red was release into the aqueous medium.

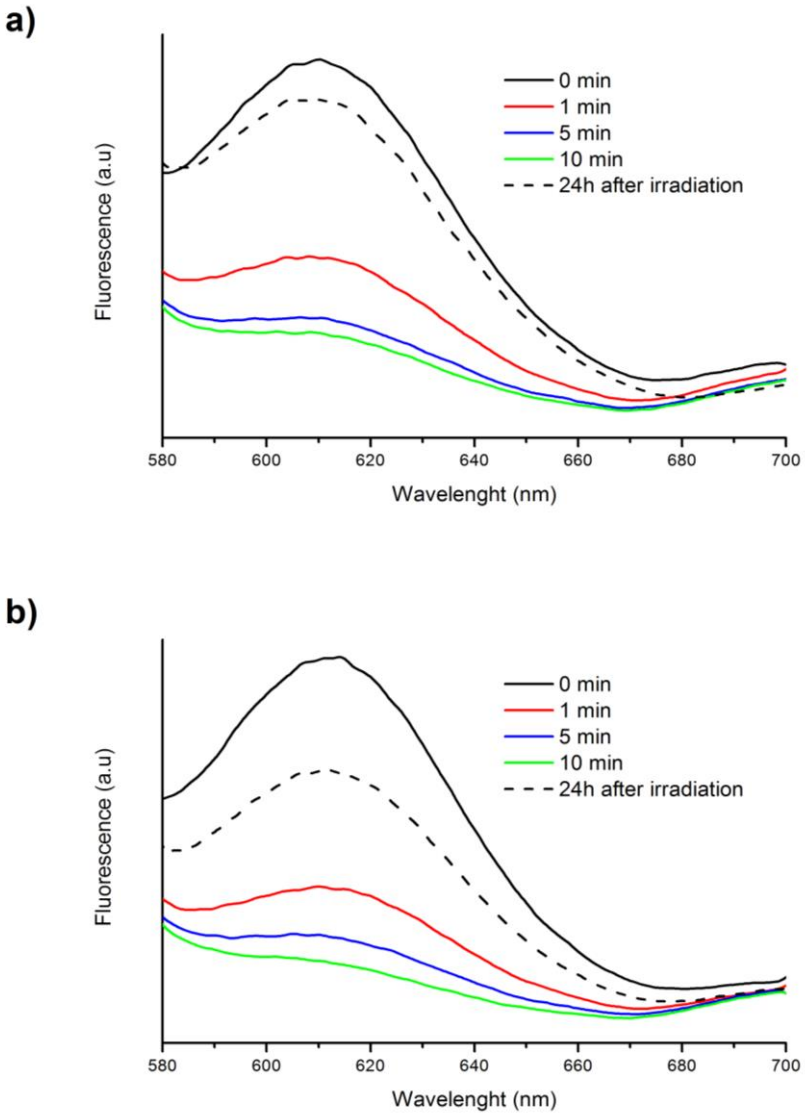

Figure 11. Emission spectra of the Nile Red encapsulated self-assemblies of (a) **{PEG$_2$-*b*-PDAP•tAZO$_i$}** and (b) **{PEG$_{10}$-*b*-PDAP•tAZO$_i$}** recorded after irradiation for different time intervals.

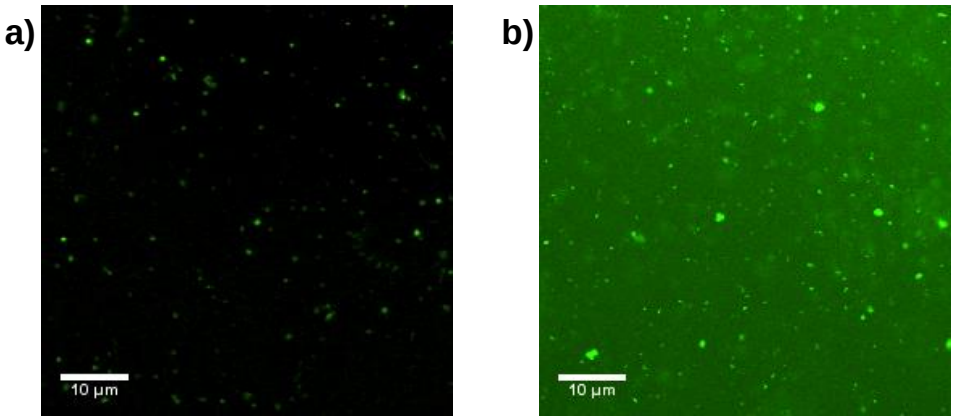

Figure 12. Fluorescence microscopy images of the water suspension of loaded **{PEG$_2$-*b*-PDAP•tAZO$_i$}** vesicles **(a)** before and **(b)** after irradiation for 10 min.

CONCLUSIONS

The aqueous behavior of supramolecular amphiphilic BCs based on the H-bond complexation of side chain 2,6-diacylaminopyridine units with thymine functionalized 4-isobutyloxybenzene is described. These supramolecular BCs, in which PEG is used as the hydrophilic block, have been prepared by selectively embedding an azobenzene derivative into the hydrophobic block through triple H-bonding. While for the parent BCs, **PEG$_{10}$-*b*-PDAP** and **PEG$_2$-*b*-PDAP**, core-shell spherical micelles were formerly described,[38] spherical micellar aggregates have been obtained for the supramolecular **{PEG$_{10}$-*b*-PDAP•tAZO$_i$}** and vesicles for **{PEG$_2$-*b*-PDAP•tAZO$_i$}** upon self-assembly in water.

When triggering the *E*-to-*Z* isomerization by low intensity UV illumination of the self-assemblies aqueous suspensions, morphological changes were observed by DLS and TEM that were confirmed by on real time SAXS analysis. These morphological changes are the basis of the demonstrated release of entrapped molecular fluorescent probes establishing the potential of

these light-responsive self-assemblies as nanocarriers for transporting and stimuli delivery of bioactive molecules. For **{PEG_2-*b*-PDAP•$tAZO_i$}** vesicles**,** distortion and thinning of the vesicle wall was observed by TEM and SAXS. These light stimulated changes modify the permeability of the membrane towards guest molecules, either hydrophobic cargo molecules entrapped at the membrane or hydrophilic ones entrapped at the internal aqueous cavity. For **{PEG_{10}-*b*-PDAP•$tAZO_i$}** light provokes destruction of the core-shell micelles accompanied by the release of hydrophobic molecules entrapped at the micellar hydrophobic core.

It should be pointed out that these supramolecular systems have, in general, similar light responsive capacities to those previously obtained for some covalent amphiphilic BCs.[16, 17, 48, 49] Thus it can be concluded that this synthetic methodology is an effective and easy way to obtain stimuli responsive assemblies and avoids the time-consuming procedures associated to the preparation of covalent amphiphilic BCs.

ACKNOWLEDGEMENTS

This work was supported by the MINECO, Spain, under the project MAT2011-27978-C02-01 and MAT2014-55205, FEDER funding and Aragón Government. A. Concellón acknowledges MINECO for his PhD grant. A. Martínez-Felipe thanks the financial support of the Generalitat Valenciana for his APOSTD/2013/054 grant. The authors would like to acknowledge the Servicio General de Apoyo a la Investigación – SAI and the Advanced Microscopy Laboratory – LMA of the Universidad de Zaragoza and the Servei de Microscòpia of the Universitat Autònoma de Barcelona for the TEM and cryo-TEM observations. The authors additionally acknowledge the use of the CEQMA Services of the Universidad de Zaragoza-CSIC. The

authors also thank the IACS (Aragón Health Sciences Institute) for the confocal microscope studies.

Supporting Information. Synthesis details and characterization of **dAZOi** and **tAZOi**. ^{1}H-^{1}H NOESY spectrum of **{PEG$_2$-*b*-PDAP•tAZO$_i$}**. FTIR spectra of **{PDAP•dAZO$_i$}** and **{PDAP•tAZO$_i$}.** Self-Assembly of the supramolecular BCs in water and determination of CAC. This material is available free of charge via the Internet at http://pubs.acs.org.

Table 1. Thermal parameters obtained for the azocompounds, parent polymers and supramolecular polymers

	Degree of complexation [a]	Hydrophilic/Hydrophobic wt. ratio [b]	T_{onset} [c] (ºC)	T_g [d] (ºC)	T_m [e] (ºC)
tAZO$_i$	–	–	360	–	166
dAZO$_i$	–	–	350	68	141
PDAP	0	–	255	73	–
PEG$_2$-CTA	0	–	210	–	48
PEG$_2$-*b*-PDAP	0	35/65	250	6	–
PEG$_{10}$-CTA	0	–	310	–	58
PEG$_{10}$-*b*-PDAP	0	37/63	255	-3	–
{PDAP • tAZO$_i$}	1	–	265	35	148
{PEG$_2$-*b*-PDAP • tAZO$_i$}	1	18/82	250	33	40, 140
{PEG$_{10}$-*b*-PDAP • tAZO$_i$}	1	19/81	270	38	48, 146
{PDAP • dAZO$_i$}	1	–	270	77	136
{PEG$_2$-*b*-PDAP • dAZO$_i$}	0.30	20/80	255	4, 80	40, 139
{PEG$_{10}$-*b*-PDAP • dAZO$_i$}	0.30	20/80	265	15, 79	52, 140

a Number of tAZOi or dAZOi molecules per 2,6-diacylaminopyridine repeating unit

b Hydrophobic/hydrophilic ratio is given in weight percentage considering the PEG block as hydrophilic the PDAP block (complexed with dAZOi or tAZOi) as hydrophobic.

c Onset temperature associated to mass loss detected in the thermogravimetric curve

d Glass transition temperature determined at the half height of the baseline jump on the second heating scan at 10 ºC min-1

e Melting temperature(s) read at the maximum of the peak on the second heating scan at 10 ºC min^{-1}

REFERENCES

1. Riess, G. *Prog. Polym. Sci.* **2003,** *28*, (7), 1107-1170.

2. Letchford, K.; Burt, H. *Eur. J. Pharm. Biopharm.* **2007,** *65*, (3), 259-269.

3. Smart, T.; Lomas, H.; Massignani, M.; Flores-Merino, M. V.; Perez, L. R.; Battaglia, G. *Nano Today* **2008,** *3*, (3–4), 38-46.

4. Blanazs, A.; Armes, S. P.; Ryan, A. J. *Macromol. Rapid Commun.* **2009,** *30*, (4-5), 267-277.

5. Mai, Y.; Eisenberg, A. *Chem. Soc. Rev.* **2012,** *41*, (18), 5969-5985.

6. Onaca, O.; Enea, R.; Hughes, D. W.; Meier, W. *Macromol. Biosci.* **2009,** *9*, (2), 129-139.

7. Meng, F.; Zhong, Z.; Feijen, J. *Biomacromolecules* **2009,** *10*, (2), 197-209.

8. Li, M.-H.; Keller, P. *Soft Matter* **2009,** *5*, (5), 927-937.

9. Zhao, Y. *J. Mater. Chem.* **2009,** *19*, (28), 4887-4895.

10. Fomina, N.; Sankaranarayanan, J.; Almutairi, A. *Adv. Drug Deliv. Rev.* **2012,** *64*, (11), 1005-1020.

11. Gohy, J.-F.; Zhao, Y. *Chem. Soc. Rev.* **2013,** *42*, (17), 7117-7129.

12. Blasco, E.; Piñol, M.; Oriol, L. *Macromol. Rapid Commun.* **2014,** *35*, (12), 1090-1115.

13. del Barrio, J.; Oriol, L.; Sanchez, C.; Luis Serrano, J.; Di Cicco, A.; Keller, P.; Li, M.-H. *J. Am. Chem. Soc.* **2010,** *132*, (11), 3762-3769.

14. Lin, Y.-L.; Chang, H.-Y.; Sheng, Y.-J.; Tsao, H.-K. *Macromolecules* **2012,** *45*, (17), 7143-7156.

15. Tong, X.; Wang, G.; Soldera, A.; Zhao, Y. *J. Phys. Chem. B* **2005,** *109*, (43), 20281-20287.

16. Blasco, E.; del Barrio, J.; Sánchez-Somolinos, C.; Piñol, M.; Oriol, L. *Polym. Chem.* **2013,** *4*, (7), 2246-2254.

17. Blasco, E.; Serrano, J. L.; Piñol, M.; Oriol, L. *Macromolecules* **2013,** *46*, (15), 5951-5960.

18. Dong, R.; Zhou, Y.; Huang, X.; Zhu, X.; Lu, Y.; Shen, J. *Adv. Mater.* **2015,** *27*, (3), 498-526.

19. Wang, D.; Tong, G.; Dong, R.; Zhou, Y.; Shen, J.; Zhu, X. *Chem. Commun.* **2014,** *50*, (81), 11994-12017.

20. Kato, T.; Fréchet, J. M. J. *Macromolecules* **1989,** *22*, (9), 3818-3819.

21. Fouquey, C.; Lehn, J. M.; Levelut, A. M. *Adv. Mater.* **1990,** *2*, (5), 254-257.

22. Brunsveld, L.; Folmer, B. J. B.; Meijer, E. W.; Sijbesma, R. P. *Chem. Rev.* **2001,** *101*, (12), 4071-4097.

23. Lehn, J. M., Supramolecular Polymer Chemistry - Scope and Perspectives. In *Supramolecular Polymers*, Ciferri, A., Ed. Taylor & Francis Group: 2005; pp 3-28.

24. Fox, J. D.; Rowan, S. J. *Macromolecules* **2009,** *42*, (18), 6823-6835.

25. Aida, T.; Meijer, E. W.; Stupp, S. I. *Science* **2012,** *335*, (6070), 813-817.

26. Zhang, Q.; Bazuin, C. G.; Barrett, C. J. *Chem. Mater.* **2008,** *20*, (1), 29-31.

27. Marcos, M.; Alcalá, R.; Barberá, J.; Romero, P.; Sánchez, C.; Serrano, J. L. *Chem. Mater.* **2008,** *20*, (16), 5209-5217.

28. Hernández-Ainsa, S.; Alcalá, R.; Barberá, J.; Marcos, M.; Sánchez, C.; Serrano, J. L. *Macromolecules* **2010,** *43*, (6), 2660-2663.

29. Hernández-Ainsa, S.; Alcalá, R.; Barberá, J.; Marcos, M.; Sánchez, C.; Serrano, J. L. *Eur. Polym. J.* **2011,** *47*, (3), 311-318.

30. Priimagi, A.; Vapaavuori, J.; Rodríguez, F. J.; Faul, C. F. J.; Heino, M. T.; Ikkala, O.; Kauranen, M.; Kaivola, M. *Chem. Mater.* **2008,** *20*, (20), 6358-6363.

31. Vapaavuori, J.; Priimagi, A.; Kaivola, M. *J. Mater. Chem.* **2010,** *20*, (25), 5260-5264.

32. Vapaavuori, J.; Valtavirta, V.; Alasaarela, T.; Mamiya, J.-I.; Priimagi, A.; Shishido, A.; Kaivola, M. *J. Mater. Chem.* **2011,** *21*, (39), 15437-15441.

33. Vapaavuori, J.; Mahimwalla, Z.; Chromik, R. R.; Kaivola, M.; Priimagi, A.; Barrett, C. J. *J. Mater. Chem. C* **2013,** *1*, (16), 2806-2810.

34. Koskela, J. E.; Vapaavuori, J.; Ras, R. H. A.; Priimagi, A. *ACS Macro Lett.* **2014,** *3*, (11), 1196-1200.

35. del Barrio, J.; Blasco, E.; Oriol, L.; Alcalá, R.; Sánchez-Somolinos, C. *J. Polym. Sci. Part A: Polym. Chem.* **2013,** *51*, (8), 1716-1725.

36. del Barrio, J.; Blasco, E.; Toprakcioglu, C.; Koutsioubas, A.; Scherman, O. A.; Oriol, L.; Sánchez-Somolinos, C. *Macromolecules* **2014,** *47*, (3), 897-906.

37. Concellón, A.; Blasco, E.; Piñol, M.; Oriol, L.; Díez, I.; Berges, C.; Sánchez-Somolinos, C.; Alcalá, R. *J. Polym. Sci. Part A: Polym. Chem.* **2014,** *52*, (22), 3173-3184.

38. Concellón, A.; Clavería-Gimeno, R.; Velázquez-Campoy, A.; Abián, O.; Piñol, M.; Oriol, L. *RSC Adv.* **2016,** *6*, (29), 24066-24075.

39. Balta Calleja, F. J.; Vonk, C. G., *X-ray scattering of synthetic polymers*. Elsevier: Amsterdam, 1989; p XI, 317 p.

40. Ezquerra, T. A.; Garcia-Gutierrez, M. C.; Nogales, A.; Gómez, M. A., *Applications of synchrotron light to scattering and diffraction in materials and life sciences*. Springer-Verlag: Berlin, 2009; p 314 p.

41. Yuan, W.; Wang, J.; Li, L.; Zou, H.; Yuan, H.; Ren, J. *Macromol. Rapid Commun.* **2014,** *35*, (20), 1776-1781.

42. Rainbolt, E. A.; Washington, K. E.; Biewer, M. C.; Stefan, M. C. *Polym. Chem.* **2015,** *6*, (13), 2369-2381.

43. Pauw, B. R.; Pedersen, J. S.; Tardif, S.; Takata, M.; Iversen, B. B. *J. Appl. Crystallogr.* **2013,** *46*, (2), 365-371.

44. Bressler, I.; Pauw, B. R.; Thunemann, A. F. *J. Appl. Crystallogr.* **2015,** *48*, (3), 962-969.

45. Feigin, L. A.; Svergun, D. I., *Structure Analysis By Small Angle X-ray and Neutron Scattering*. Plenum Press: New York, 1987.

46. Pedersen, J. S.; Gerstenberg, M. C. *Macromolecules* **1996,** *29*, (4), 1363-1365.

47. Pedersen, J. S. *J. Appl. Crystallogr.* **2000,** *33*, (3-1), 637-640.

48. Blasco, E.; Schmidt, B. V. K. J.; Barner-Kowollik, C.; Piñol, M.; Oriol, L. *Polym. Chem.* **2013,** *4*, (16), 4506-4514.

49. Blasco, E.; Schmidt, B. V. K. J.; Barner-Kowollik, C.; Piñol, M.; Oriol, L. *Macromolecules* **2014,** *47*, (11), 3693-3700.

TABLE OF CONTENTS GRAPHIC

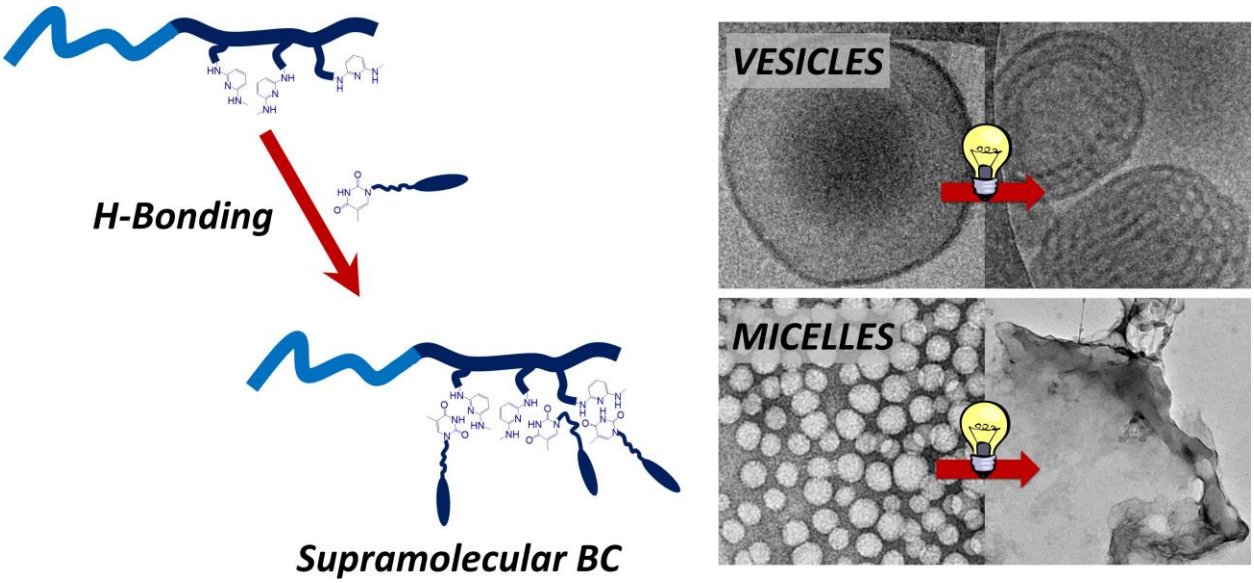

KEYWORDS

Amhiphilic block copolymers; suparamolecular post-functionalization; light-responsive nanoself-assemblies